U.S. DEPARTMENT OF THE INTERIOR

U.S. GEOLOGICAL SURVEY

BOREHOLE VELOCITY MEASUREMENTS AT FIVE SITES THAT RECORDED THE CAPE MENDOCINO, CALIFORNIA EARTHQUAKE OF 25 APRIL, 1992

by

James F. Gibbs[1], John C. Tinsley[1], and David M. Boore[1]

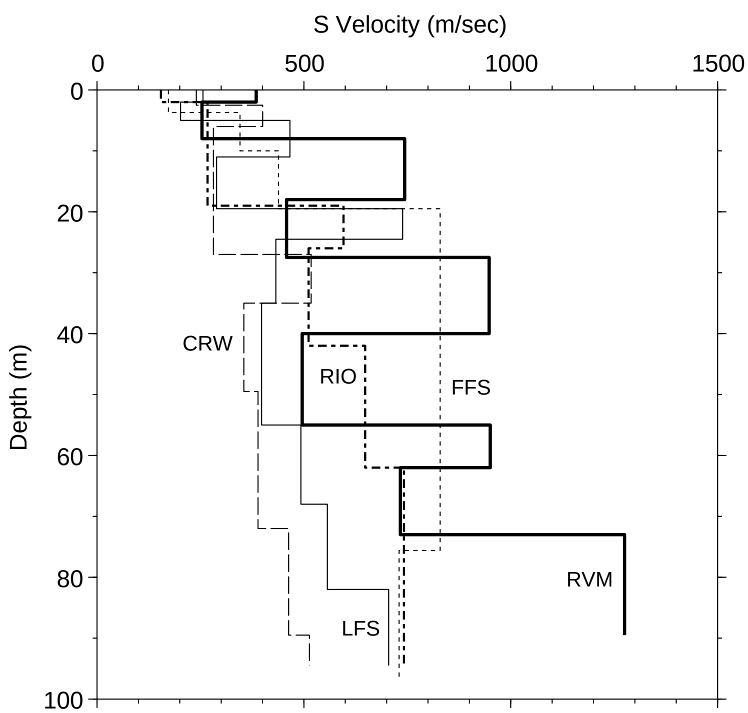

U.S. Geological Survey Open-File Report OF 02-203

[1]Menlo Park, CA 94025

U.S. DEPARTMENT OF THE INTERIOR
U.S. GEOLOGICAL SURVEY

BOREHOLE VELOCITY MEASUREMENTS AT FIVE SITES THAT RECORDED THE CAPE MENDOCINO, CALIFORNIA EARTHQUAKE OF 25 APRIL, 1992

by

James F. Gibbs[1], John C. Tinsley[1], and David M. Boore[1]

U.S. Geological Survey Open-File Report OF 02-203

[1]Menlo Park, CA 94025

TABLE OF CONTENTS

BOREHOLE VELOCITY MEASUREMENTS AT FIVE SITES THAT RECORDED THE CAPE MENDOCINO, CALIFORNIA EARTHQUAKE OF 25 APRIL, 1992

by

James F. Gibbs, John C. Tinsley, and David M. Boore

INTRODUCTION

The U.S. Geological Survey (USGS), as part of an ongoing program to aquire seismic velocity and geologic data at locations that recorded strong-ground motion during earthquakes, has investigated five sites in the Fortuna, California region (Figure 1). We selected drill sites at strong-motion stations that recorded high accelerations (Table 1) from the Cape Mendocino earthquake (**M** 7.0) of 25 April 1992 (Oppenheimer *et al.*, 1993). The boreholes were drilled to a nominal depth of 95 meters (310 ft.) and cased with schedule 80 pvc-casing grouted in place at each location. S-wave and P-wave data were acquired at each site using a surface source and a borehole three-component geophone. This report contains the velocity models interpreted from the borehole data and gives reference to locations and peak accelerations at the selected strong-motion stations.

P- AND *S*-WAVE TRAVEL-TIME DATA

Shear waves were generated at the ground surface by an air-powered horizontal ram (Liu *et al.*, 1988) striking an anvil at either end of an aluminum channel 2.3 m long. The ram was driven first in one direction and then in the other to generate pulses of opposite polarity. A switch attached to the shear source triggered the recorder and established the reference for the timing of arrivals. *P*-waves were generated by striking a steel plate with a sledge hammer. The recorder was triggered by a switch attached to the handle of the sledge hammer. *P*- and *S*-wave sources were offset from the borehole (same horizontal distance but different locations) to minimize the effect of waves traveling down the grout surrounding the casing. The source offset was 4 meters except at Rio Dell where available space limited the offset to 3.5 meters. These offsets are shown in the data tables.

Downhole measurements were made at 2.5 m intervals (starting at 2 meters depth) with a three-component geophone clamped to the casing by an electrically-activated lever arm. A second three-component geophone was placed on the surface 5 to 10 m from the shear source for recording an on-scale reference trace (useful for amplitude studies and timing verification). The data were recorded on diskettes using a 12-channel recording system.

VELOCITY PROFILES

The procedure for determining velocities is summarized in Figure 2. Because the orientation of the downhole geophone could not be controlled when moving from one depth to the next, the azimuth of the horizontal geophones relative to the source was unknown and changed with depth. To minimize the effects of those changes, the horizontal components were rotated to the direction that maximized the integral square amplitude within a time interval containing the shear wave (Boatwright *et al.*, 1986). *P*- and *S*-wave first-arrival times were determined from the time series displayed at each depth on a 20-inch computer screen. The *P*-wave arrival-time was obtained from the vertical trace, and the *S*-wave

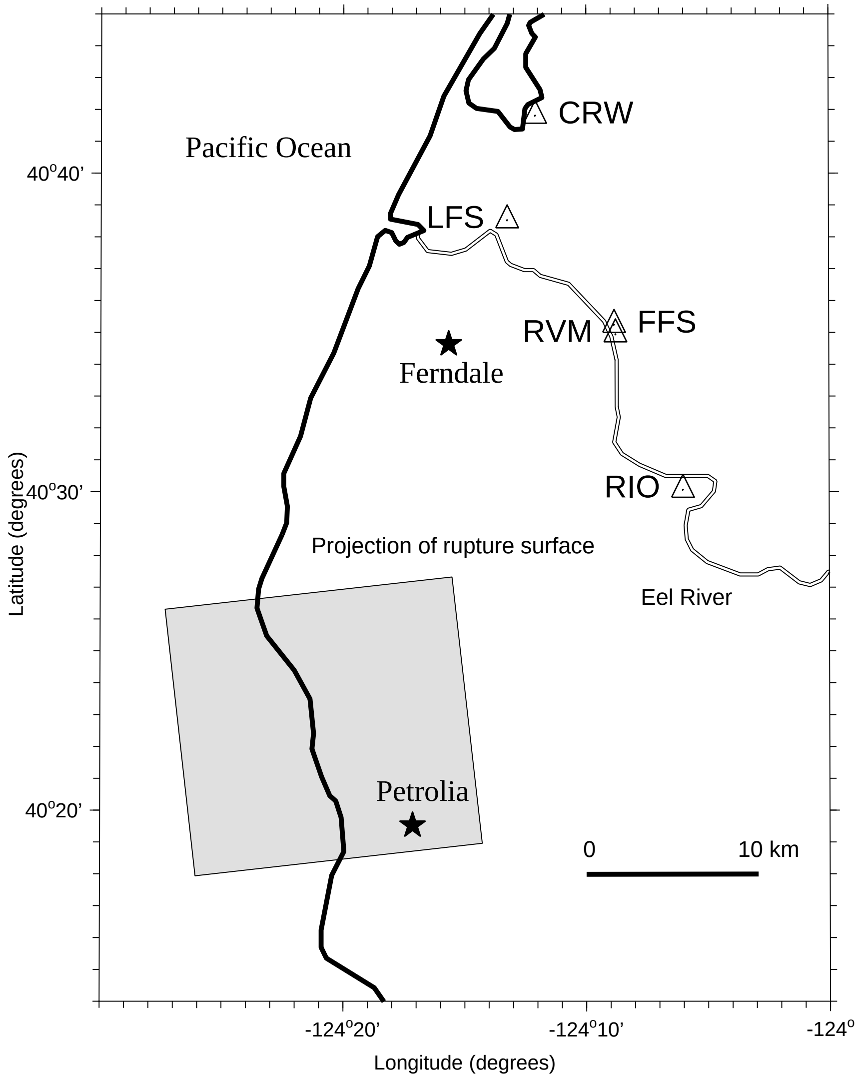

Figure 1. Regional map showing the locations of boreholes (triangles) included in this report. LFS and RIO are in the towns of Loleta and Rio Dell, respectively, and RVM and FFS are in the town of Fortuna. Locations of river and coastline are approximate. The projection of the fault rupture for the 1992 Cape Mendocino mainshock (shaded) corresponds to model B of Murray *et al.* (1996).

Table 1. Site names, station codes, coordinates using North American Datum of 1927 (NAD27) and 1983 (NAD83), and peak horizontal accelerations.

Station Name	StaCode	Lat:NAD27	Long:NAD27	Lat:NAD83	Long:NAD83	pga (cm/s^2)
College of the Redwoods	CRW	40.69913	-124.20045	40.69898	-124.20162	171
Fortuna Fire Station	FFS	40.58969	-124.14630	40.58954	-124.14746	349
Loleta Fire Station	LFS	40.64438	-124.21976	40.64423	-124.22093	252
Redwood Village Mall (Fortuna)	RVM	40.58472	-124.14538	40.58457	-124.14654	114
Rio Dell	RIO	40.50334	-124.09913	40.50320	-124.10029	539

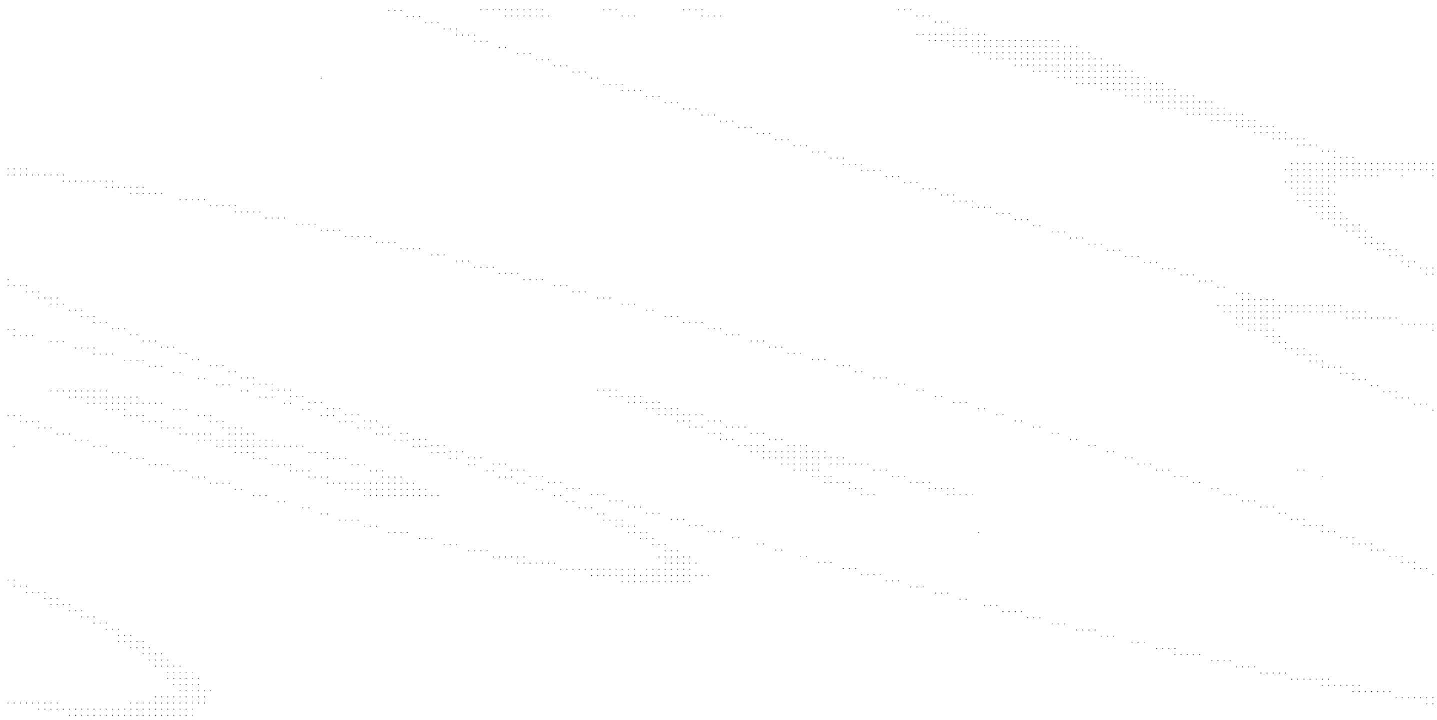

Figure 2. Flow-chart outlining the data processing and steps in the interpretation.

arrival-times were obtained from the average of the rotated horizontal traces for ram strikes in opposite directions. The arrivals were timed to the nearest millisecond, probably a realistic precision for clear arrivals uncontaminated by noise.

A trial set of layer boundaries was chosen for the S-wave model, based on the lithologic descriptions and geophysical logs. The travel-time data were fit in a least-squares sense by a model made up of constant velocity layers, taking into account refraction across the interfaces between layers. The travel times were weighted by the inverse of an assigned normalized variance. A normalized standard deviation of 1 was assigned to the clear arrivals and values up to 5 were assigned to the others. The residuals were examined, and layer boundaries were added, if necessary, to reduce large residuals or to remove systematic trends in the residuals. This was an iterative process conducted by the team of authors of this report. The process continued until the team was satisfied that the interfaces were consistent with the borehole seismic data as well as available geological and geophysical logs. The P-wave travel time data were analyzed initially with the set of layer boundaries finally determined for the S-wave data. Layer boundaries were then added if needed to fit the data and deleted if not needed. Commonly, an additional layer boundary corresponding to the top of the zone of water saturation was needed to fit the P-wave data.

Some of the dynamic Poisson's ratios σ, calculated with initial velocity models, resulted in ratios that were out of the accepted range of values (0.0–0.5). To obtain a value in the acceptable range we made minor adjustments to the velocities using one or more of the following procedures: repicking shallow arrivals (usually P arrivals because small changes in P travel-times have greater effect on σ), adding a shallow layer, and/or adjusting layer thickness to ensure that Poisson's ratio was in the range 0.0–0.5. In most cases the small changes were made in the P-wave velocities at shallow depths (for more details see, Gibbs *et al.*, 2000). Overall, the changes in velocity required to produce acceptable values of σ were small and were only in a few layers.

SUMMARY VELOCITY PROFILES

Figures 3 and 4 show the S- and P-wave velocity profiles determined from the borehole measurements at the five sites. The velocity profiles are plotted at the same scale for ease of comparison.

DESCRIPTION OF APPENDICES

Appendix A contains for each site: a location map, S- and P-wave time-series records, a time-depth plot, velocity profiles with a generalized geologic log, and tables giving arrival times and velocity values. The upper and lower bounds on the velocity plots show approximate 68 percent confidence limits. The bounds are not symmetrical because they are based on the inverse velocities in the layers. Appendix B contains tables of P- and S-wave velocity models and the Poisson's ratios obtained from those models.

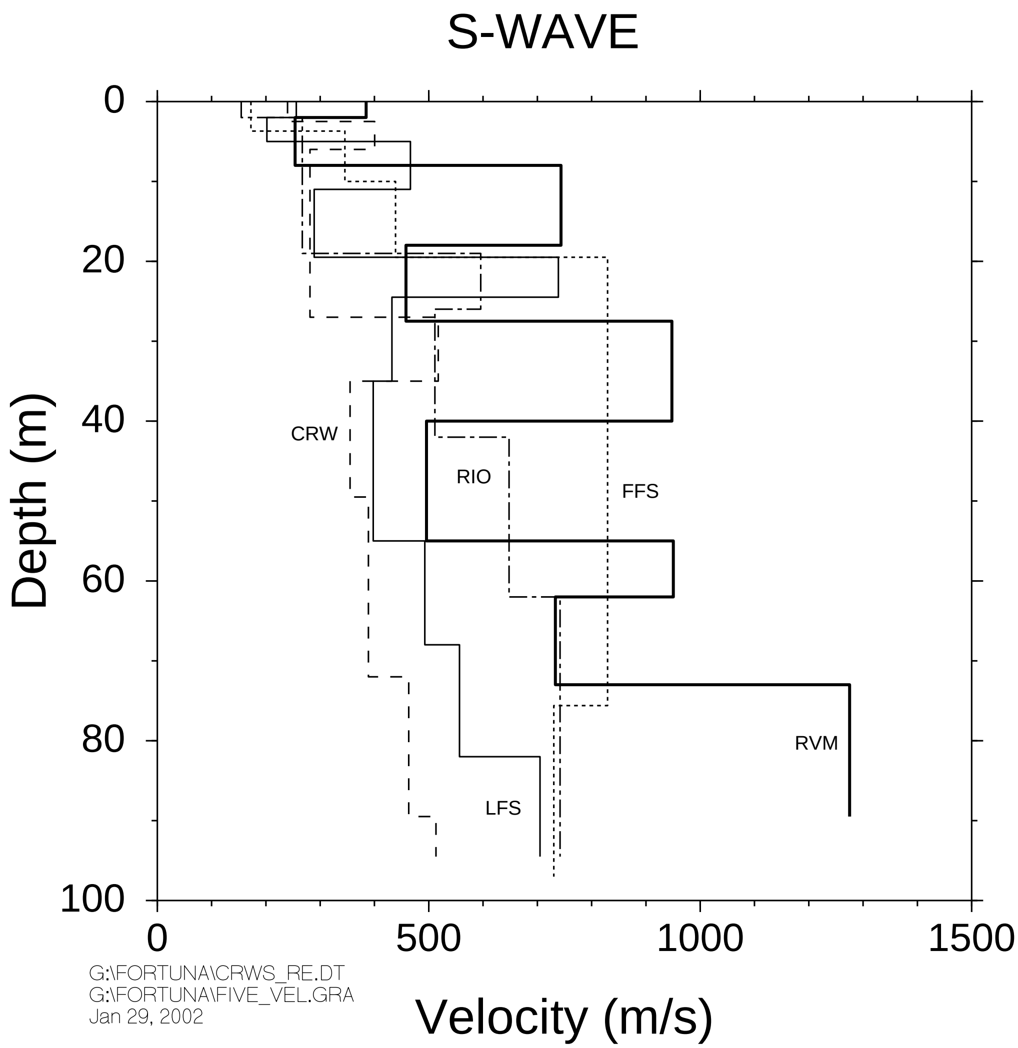

Figure 3. S-wave velocity models from all five boreholes (see Figure 1, Table 1) shown on the same figure for comparison.

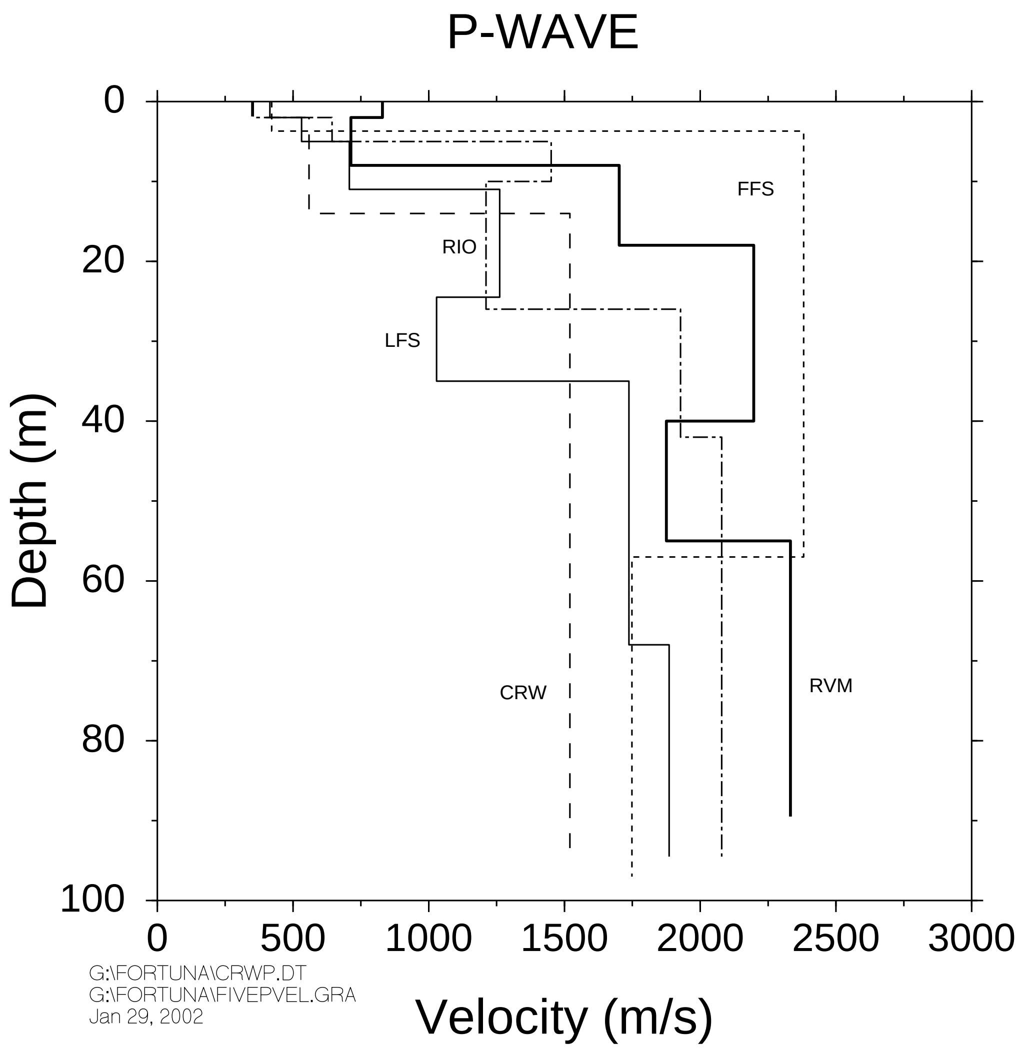

Figure 4. S-wave velocity models from all five boreholes (see Figure 1, Table 1) shown on the same figure for comparison.

ACKNOWLEDGMENTS

We could not have completed these studies without the assistance of many individuals who helped us to gain access to the sites, assisted with utilities clearances and granted permission to conduct the studies. We thank Tom Fumal for his careful review of the manuscript.

REFERENCES

Boatwright, J., R. Porcella, T. Fumal, and H.-P. Liu (1986). Direct estimates of shear wave amplification from a borehole near Coalinga, California, *Earthquake Notes* **57**, 8.

Gibbs, J.F., J.C. Tinsley, D.M. Boore, and W.B. Joyner (2000). Borehole velocity measurements and geological conditions at thirteen sites in the Los Angeles, California region, *U.S. Geol. Surv. Open-File Rept. 00-470*, 118p.

Liu, H.-P., R.E. Warrick, R.E. Westerlund, J.B. Fletcher, and G.L. Maxwell (1988). An air-powered impulsive shear-wave source with repeatable signals, *Bull. Seism. Soc. Am.* **78**, 355–369.

Oppenheimer, D., G. Beroza, G. Carver, L. Dengler, J. Eaton, L. Gee, F. Gonzalez, A. Jayko, W. H. Li, M. Lisowski, M. Magee, G. Marshall, M. Murray, R. McPherson, B. Romanowicz, K. Satake, R. Simpson, P. Somerville, R. Stein, and D. Valentine (1993). The Cape Mendocino, California, earthquakes of April 1992: Subduction at the triple junction, *Science* **261**, 433–438.

Murray, M.H., G.A. Marshall, M. Lisowski, and R.S. Stein (1996). The 1992 $M = 7$ Cape Mendocino, California, earthquake: Coseismic deformation at the south end of the Cascadia megathrust, *J. Geophys. Res.* **101**, 17,707–17,725.

APPENDIX—A

Detailed Results

Figure A-1. Site location map for the borehole at College of the Redwoods. The accelerograph is located approximately 30 meters from the borehole.

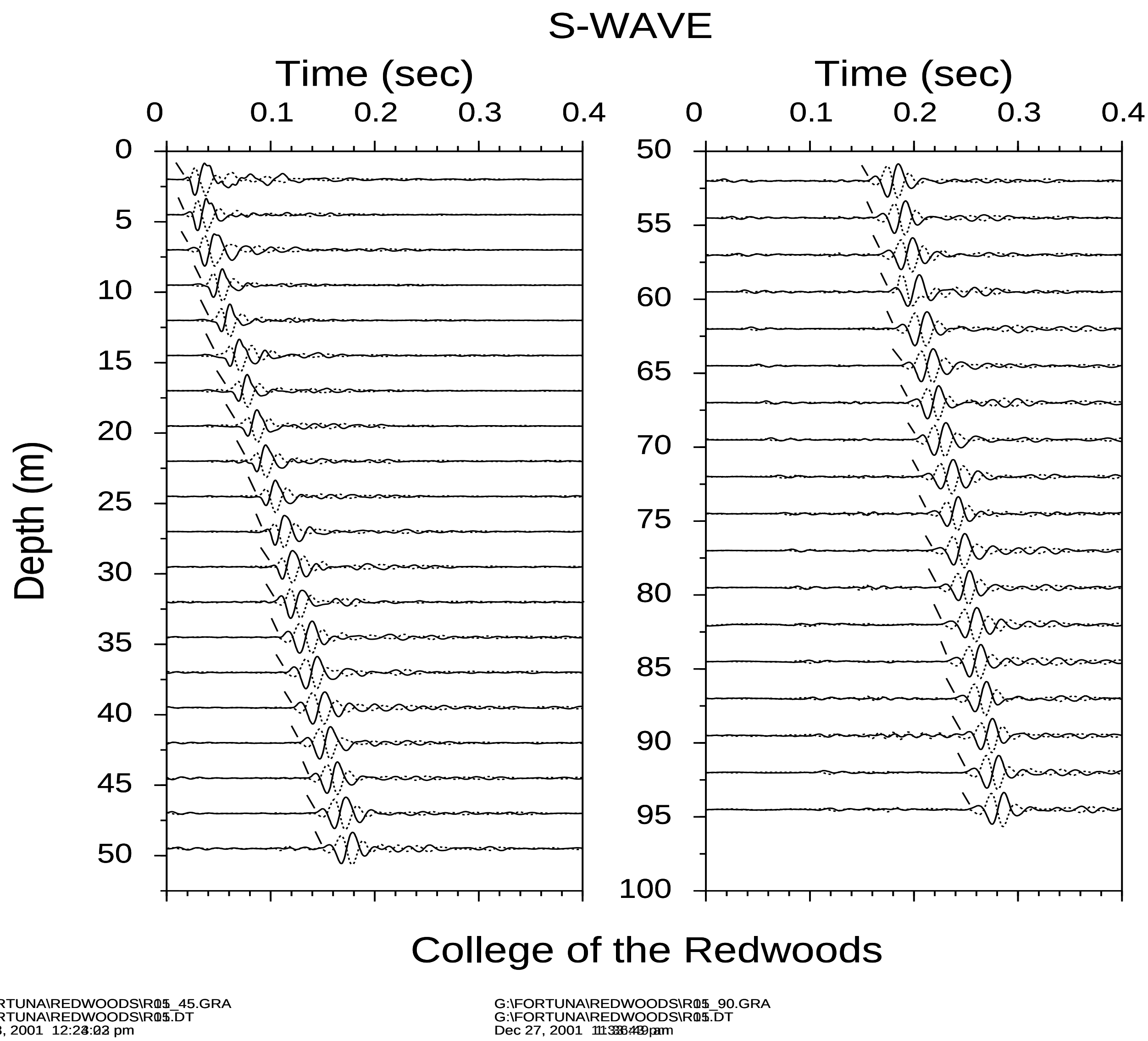

Figure A-2. Horizontal component record section (from impacts in opposite directions) superimposed for identification of S-wave onset. Approximate S-wave time picks are indicated by the hatch marks.

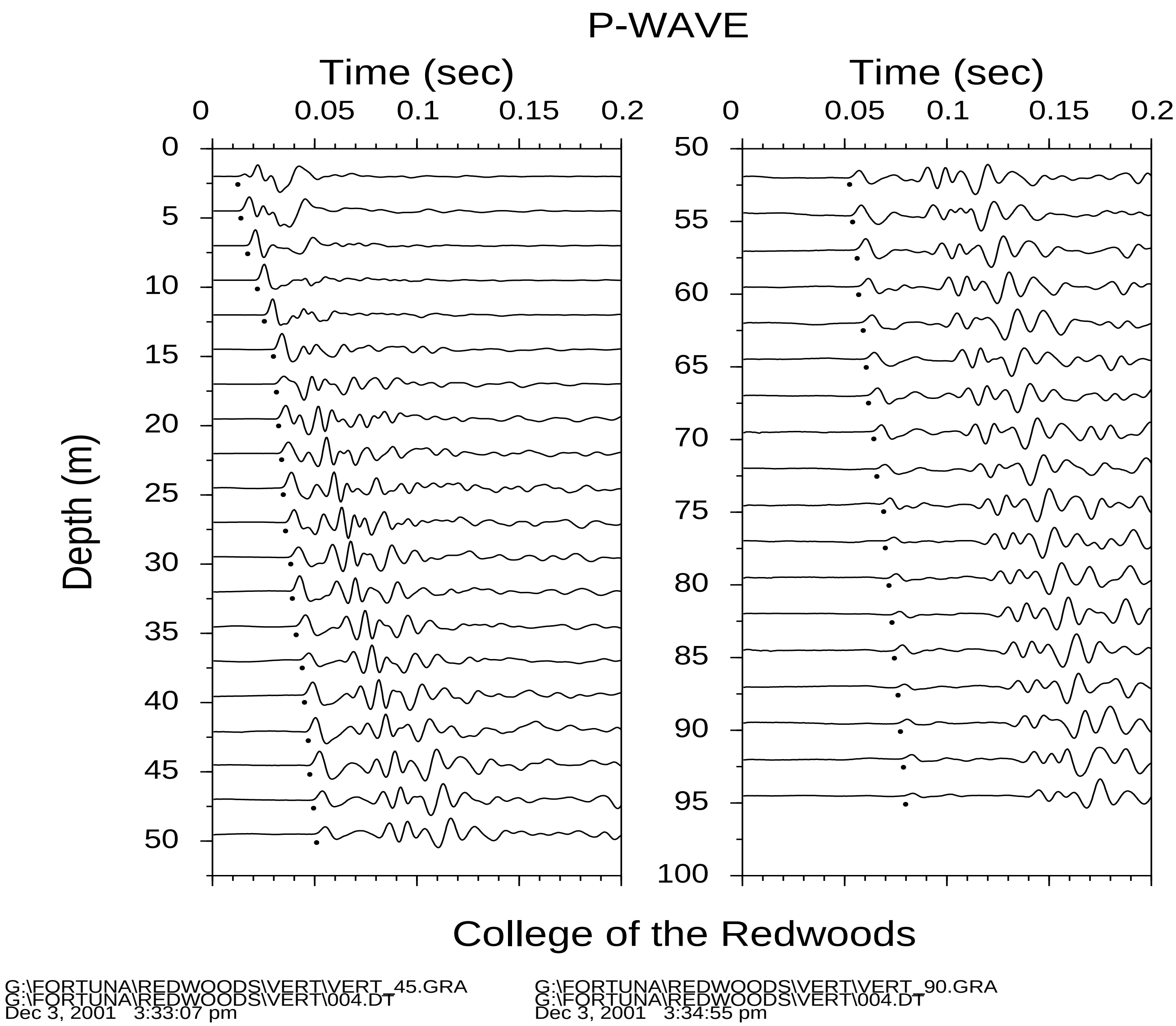

Figure A-3. Vertical component record section. Approximate P-wave arrivals are indicated by the dots.

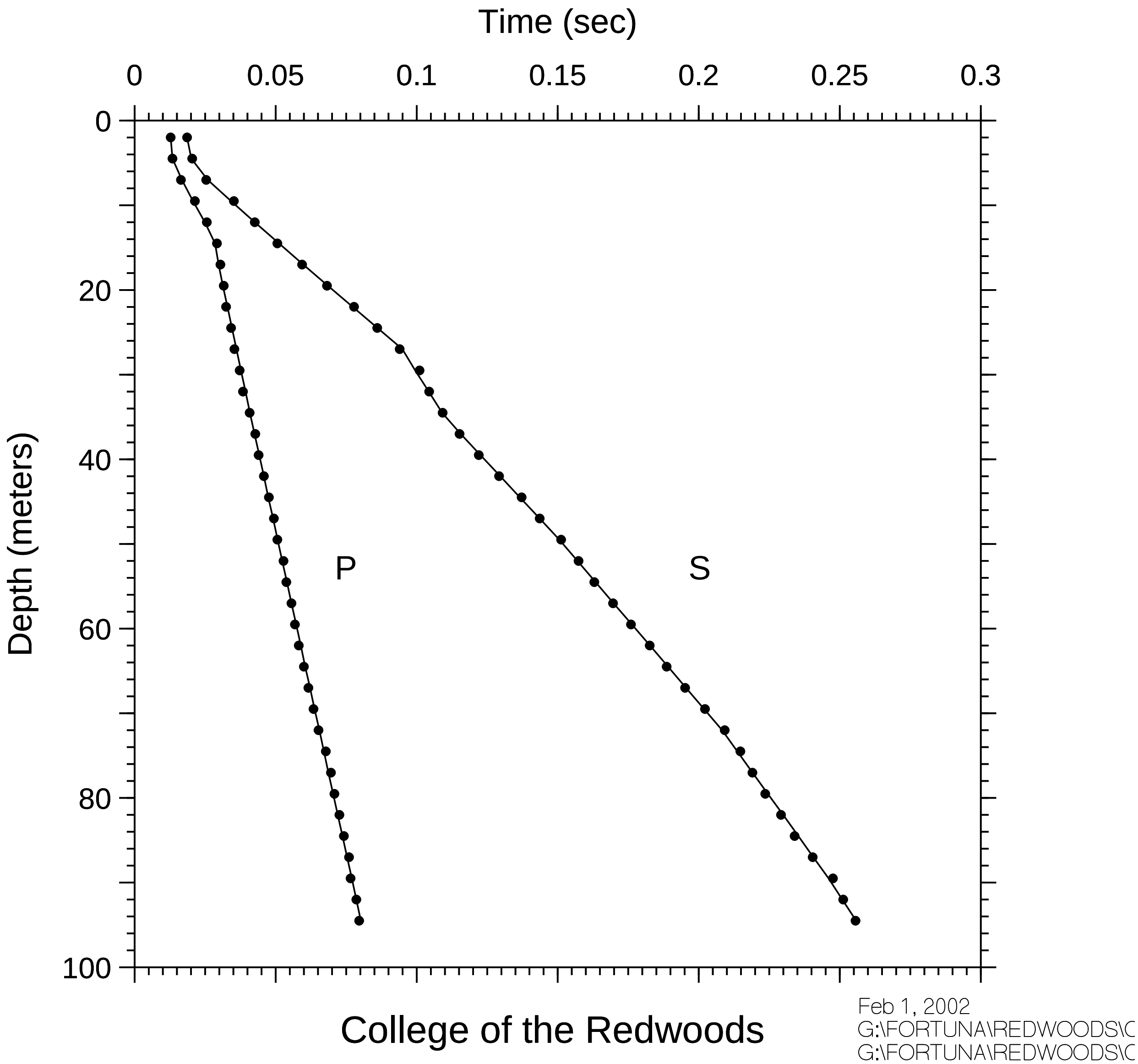

Figure A-4. Time-depth graph of P-wave and S-wave picks. Line segments are straightline interpolations of model predictions at the observation depths. The times for zero depth, not shown, are given by the horizontal offset ($hoffset$) divided by the velocity in the uppermost layer (see accompanying tables of velocities for specific values).

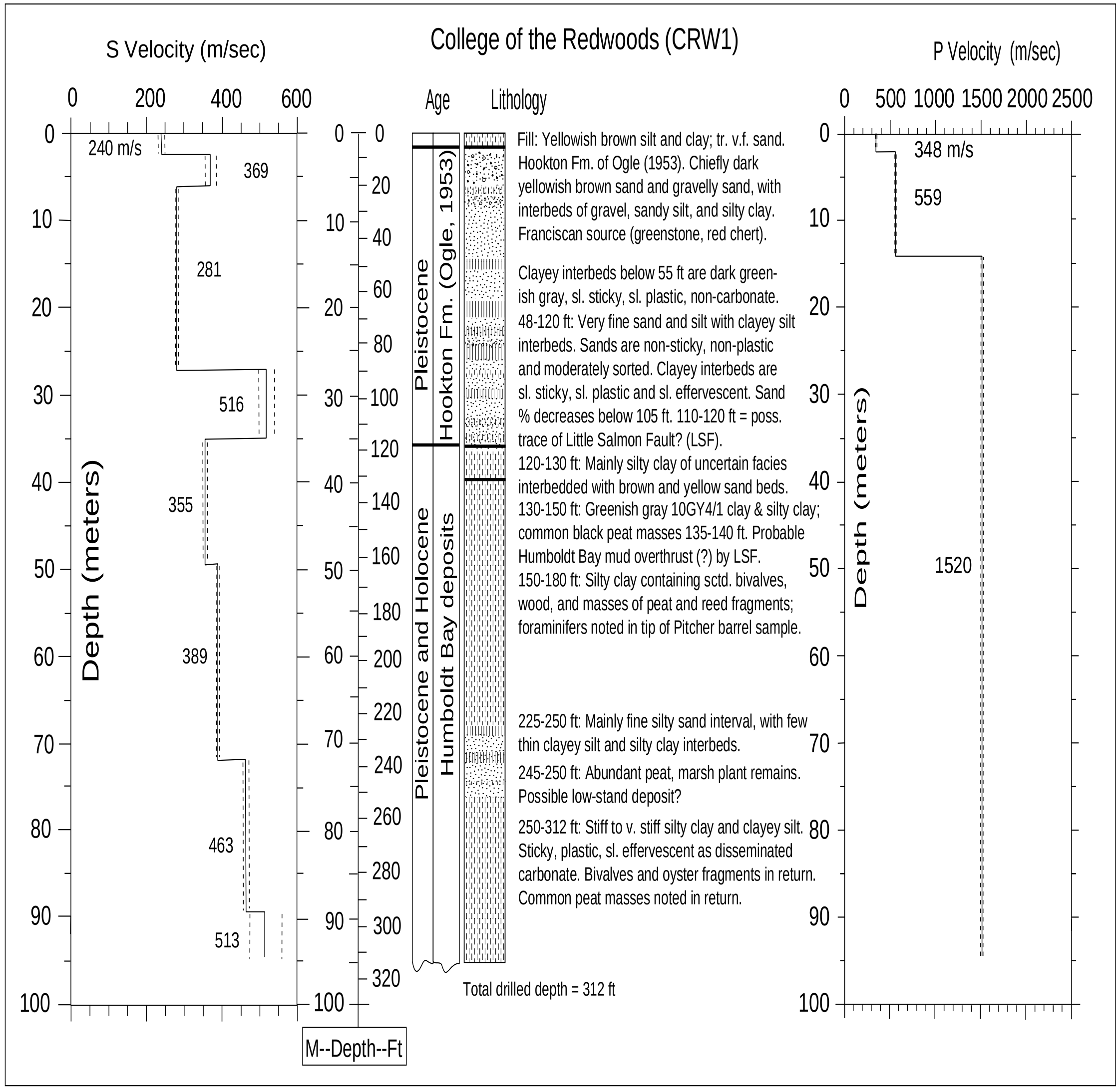

Figure A-5. S- and P-wave velocity profiles with dashed lines representing one standard deviation.

13

Figure A-6. Site location map for the borehole at Fortuna Fire Station. The accelerograph is located approximately 35 meters from the borehole.

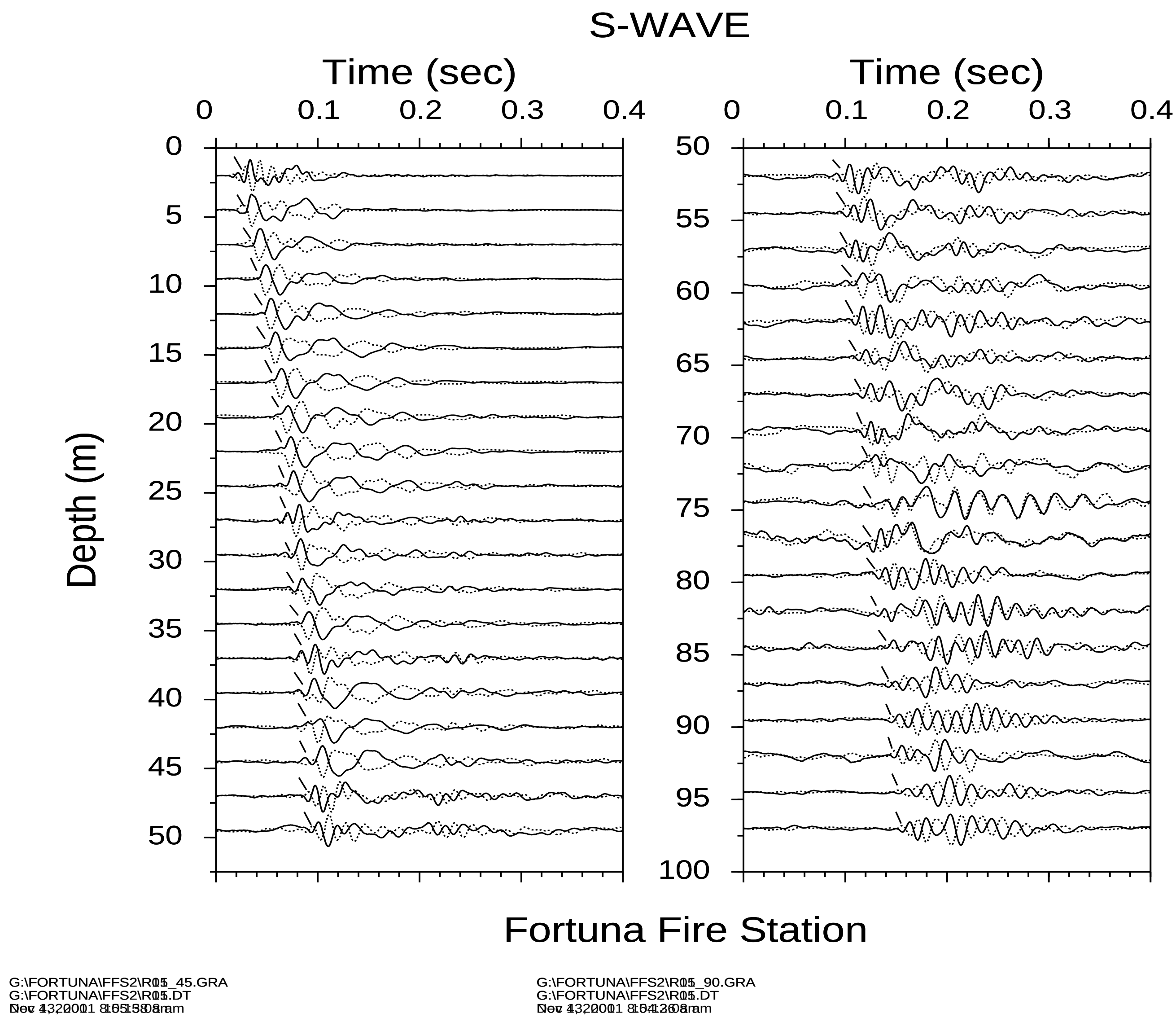

Figure A-7. Horizontal component record section (from impacts in opposite directions) superimposed for identification of S-wave onset. Approximate S-wave time picks are indicated by the hatch marks.

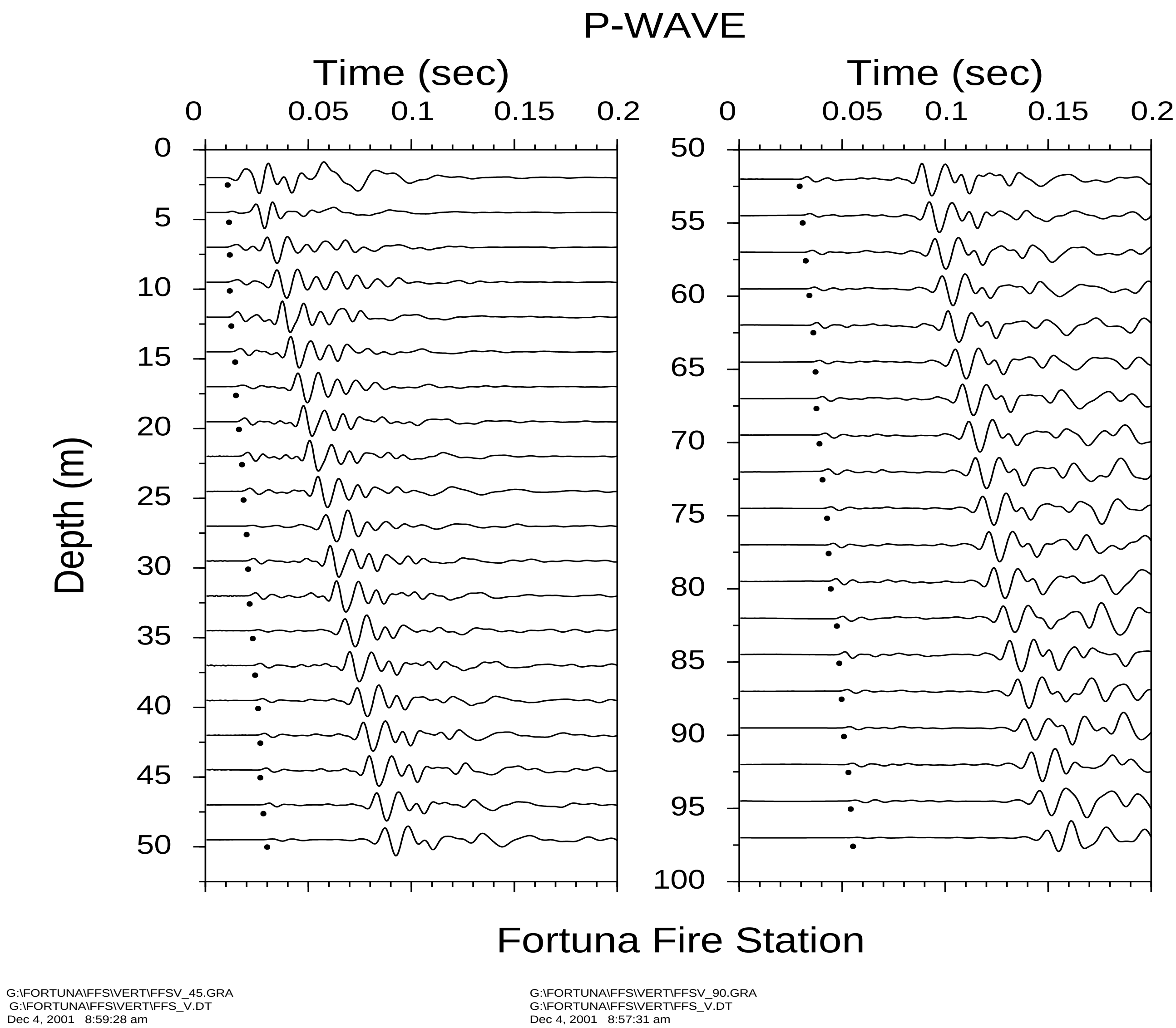

Figure A-8. Vertical component record section. Approximate P-wave arrivals are indicated by the dots.

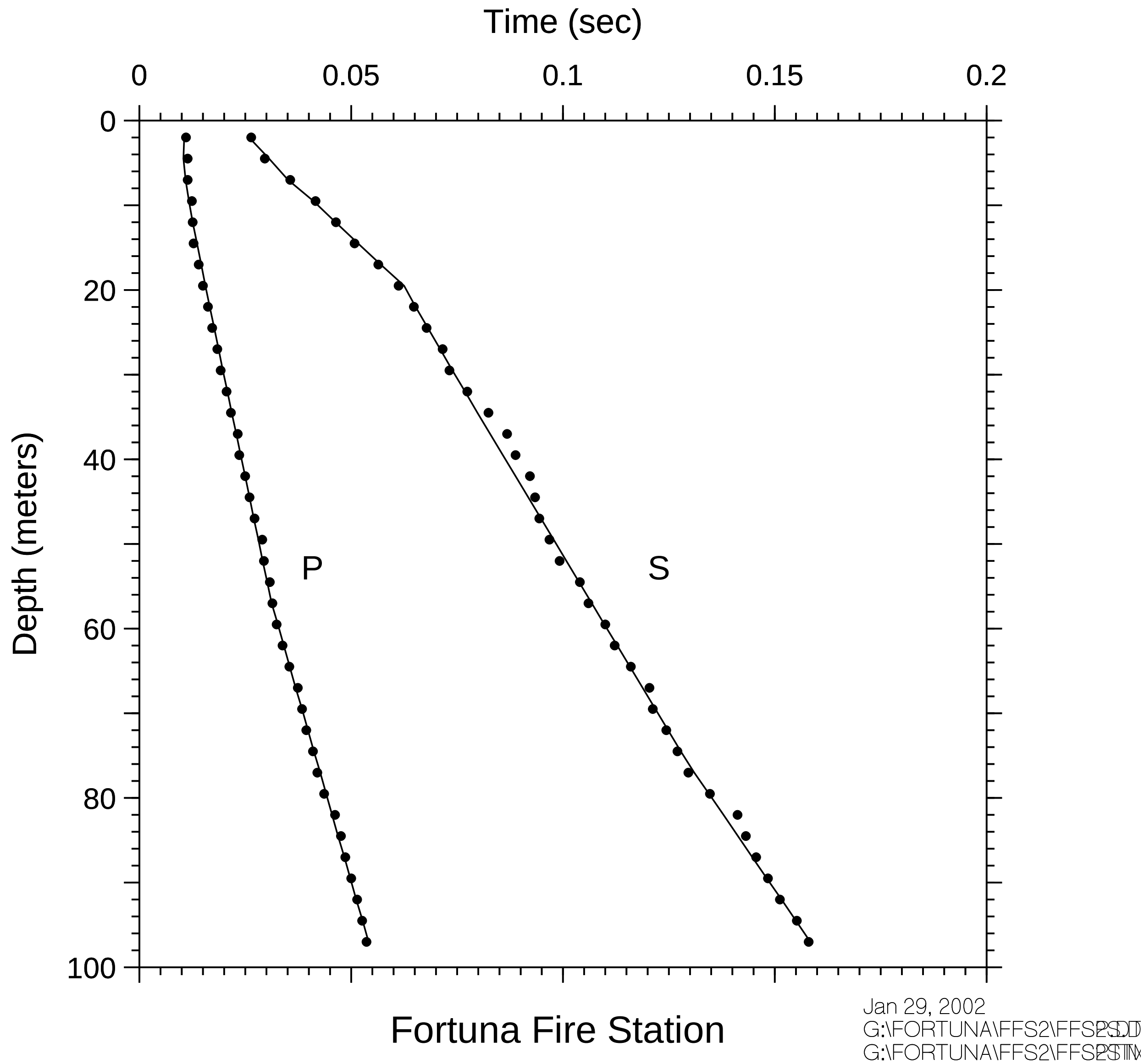

Figure A-9. Time-depth graph of P-wave and S-wave picks. Line segments are straightline interpolations of model predictions at the observation depths. For the depth intervals 37–44.5 m and 72–87 m arrival times were difficult to pick and were downweighted in fitting the model. The times for zero depth, not shown, are given by the horizontal offset ($hoffset$) divided by the velocity in the uppermost layer (see accompanying tables of velocities for specific values).

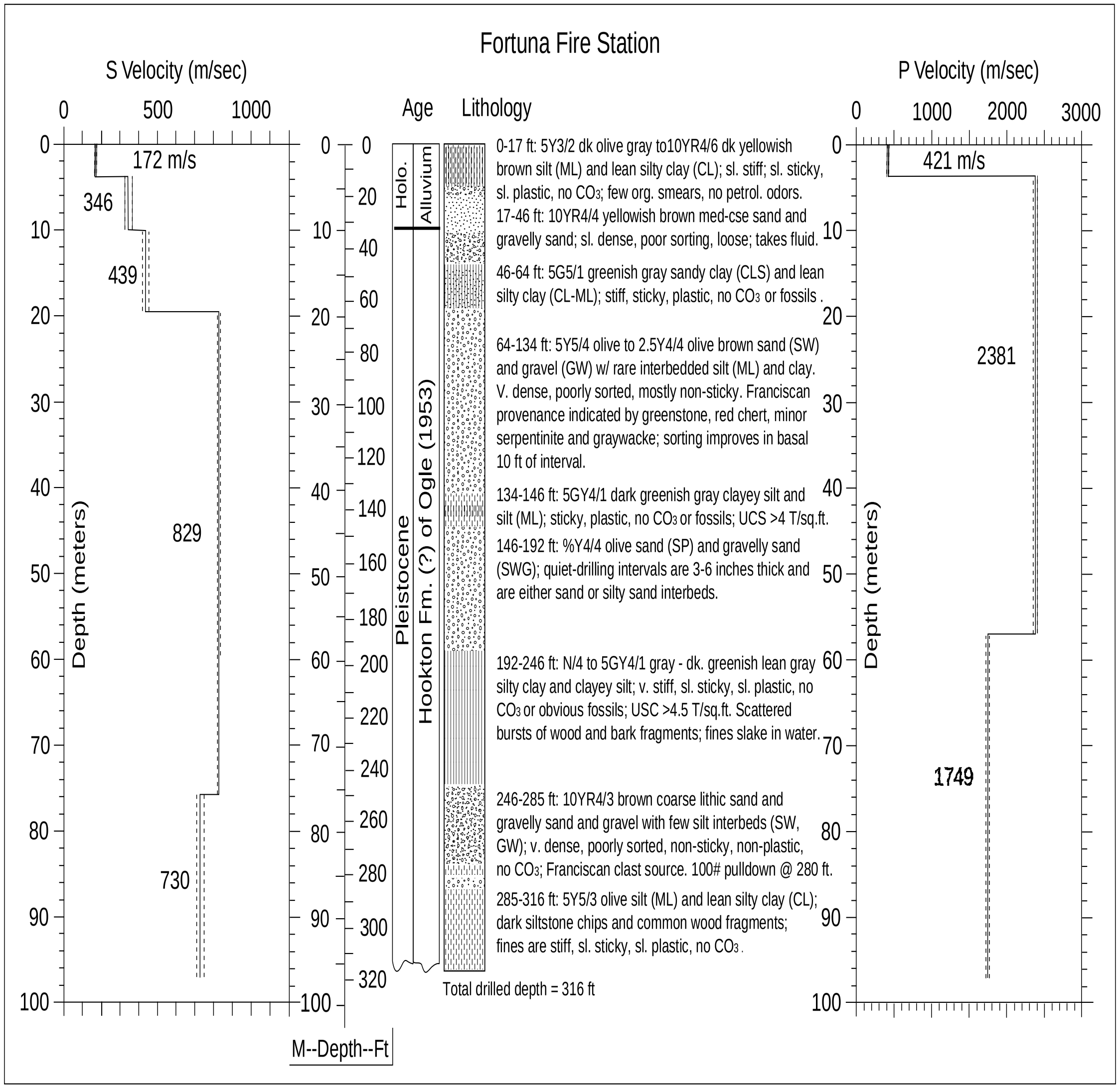

Figure A-10. S- and P-wave velocity profiles with lithology. Dashed lines represent plus and minus one standard deviation of velocities.

Figure A-1. Site location map for the borehole at Loleta Fire Station. The accelerograph is located approximately 15 meters from the borehole.

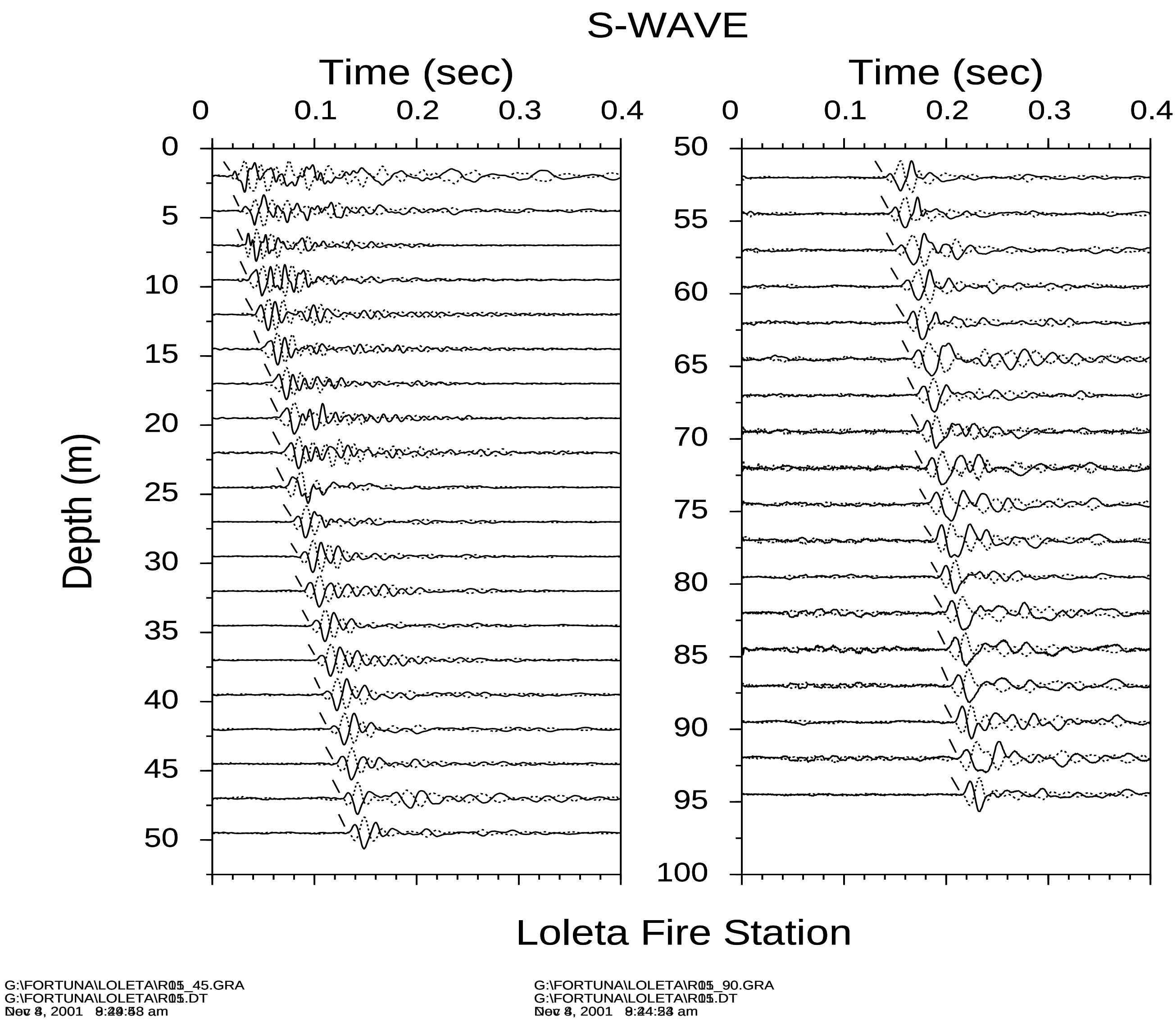

Figure A-12. Horizontal component record section (from impacts in opposite directions) superimposed for identification of S-wave onset. Approximate S-wave time picks are indicated by the hatch marks.

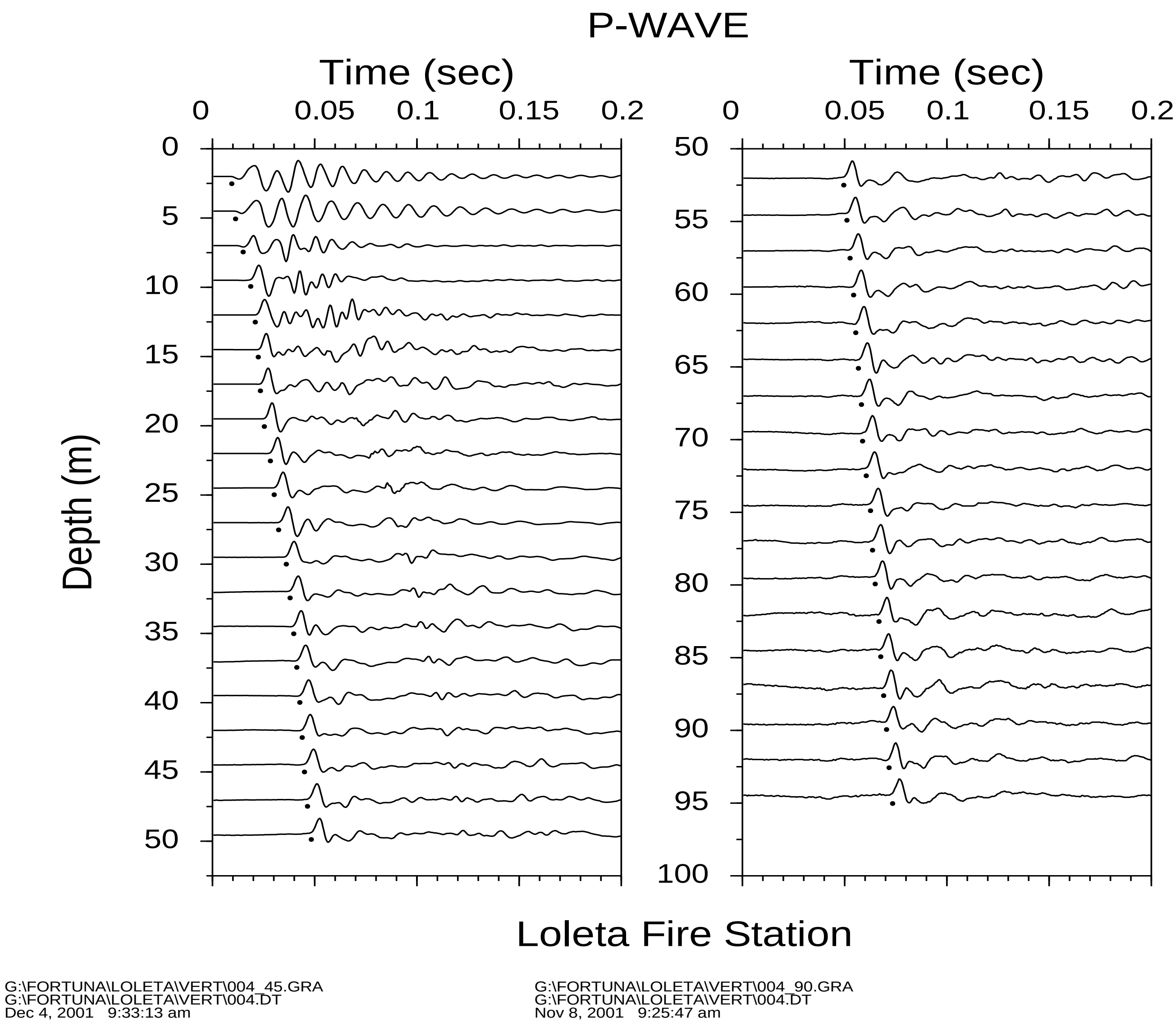

Figure A-13. Vertical component record section. Approximate P-wave arrivals are indicated by the dots.

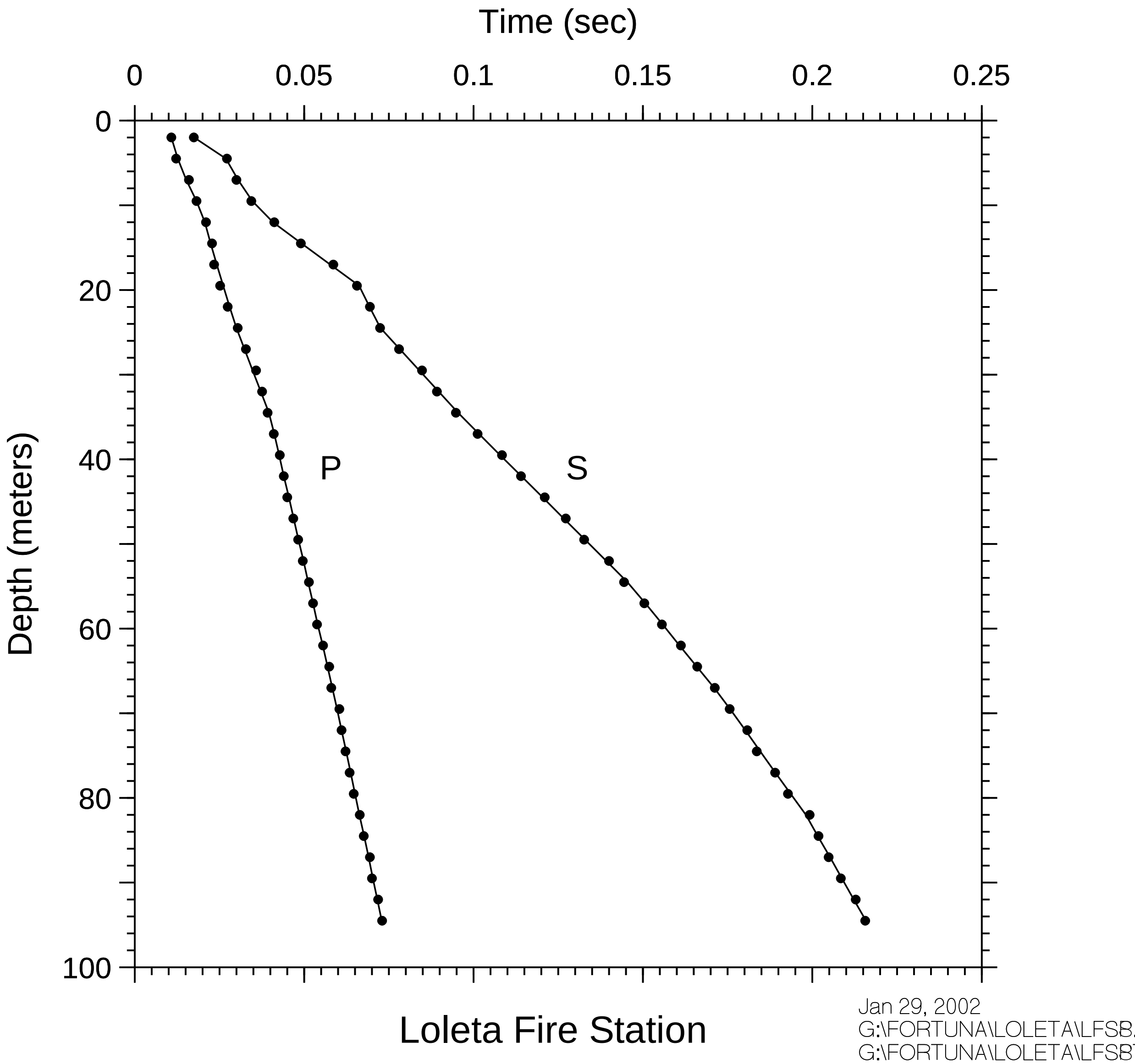

Figure A-14. Time-depth graph of P-wave and S-wave picks. Line segments are straightline interpolations of model predictions at the observation depths. The times for zero depth, not shown, are given by the horizontal offset ($hoffset$) divided by the velocity in the uppermost layer (see accompanying tables of velocities for specific values).

27

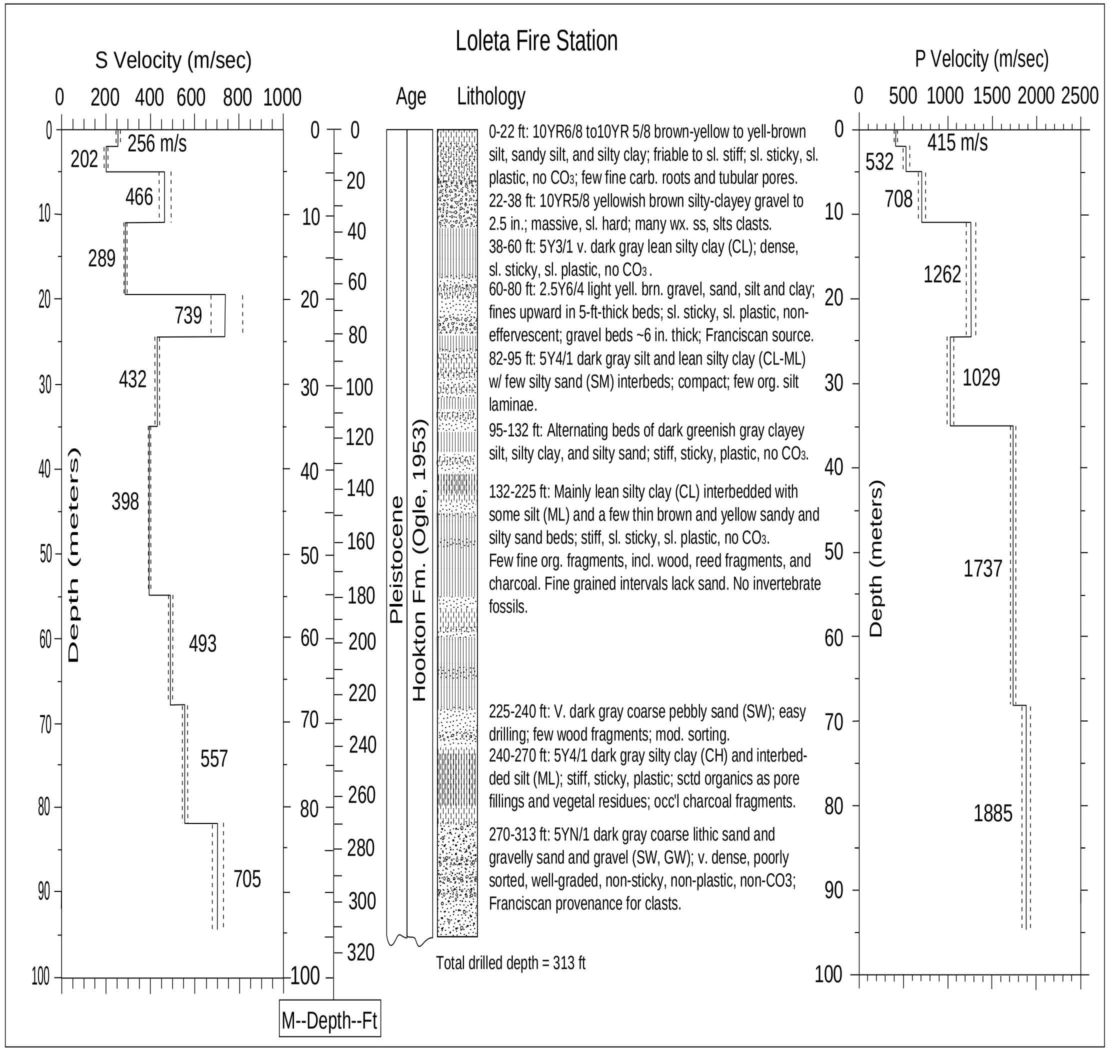

Figure A-15. S- and P-wave velocity profiles with lithology. Dashed lines represent plus and minus one standard deviation of velocities.

Figure A-16. Site location map for the borehole at Redwood Village Mall. The accelerograph is located approximately 10 meters from the borehole.

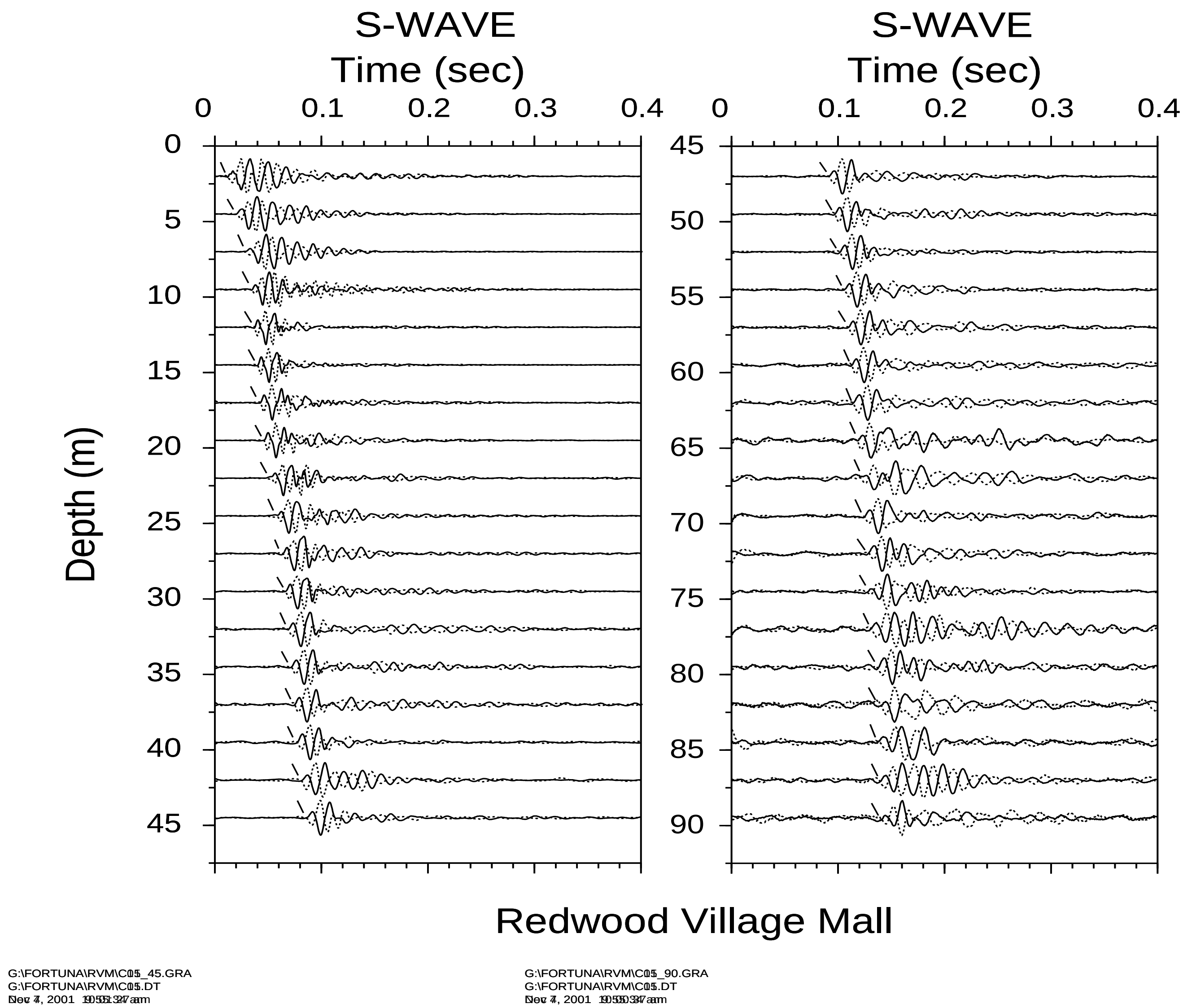

Figure A-17. Horizontal component record section (from impacts in opposite directions) superimposed for identification of S-wave onset. Approximate S-wave time picks are indicated by the hatch marks.

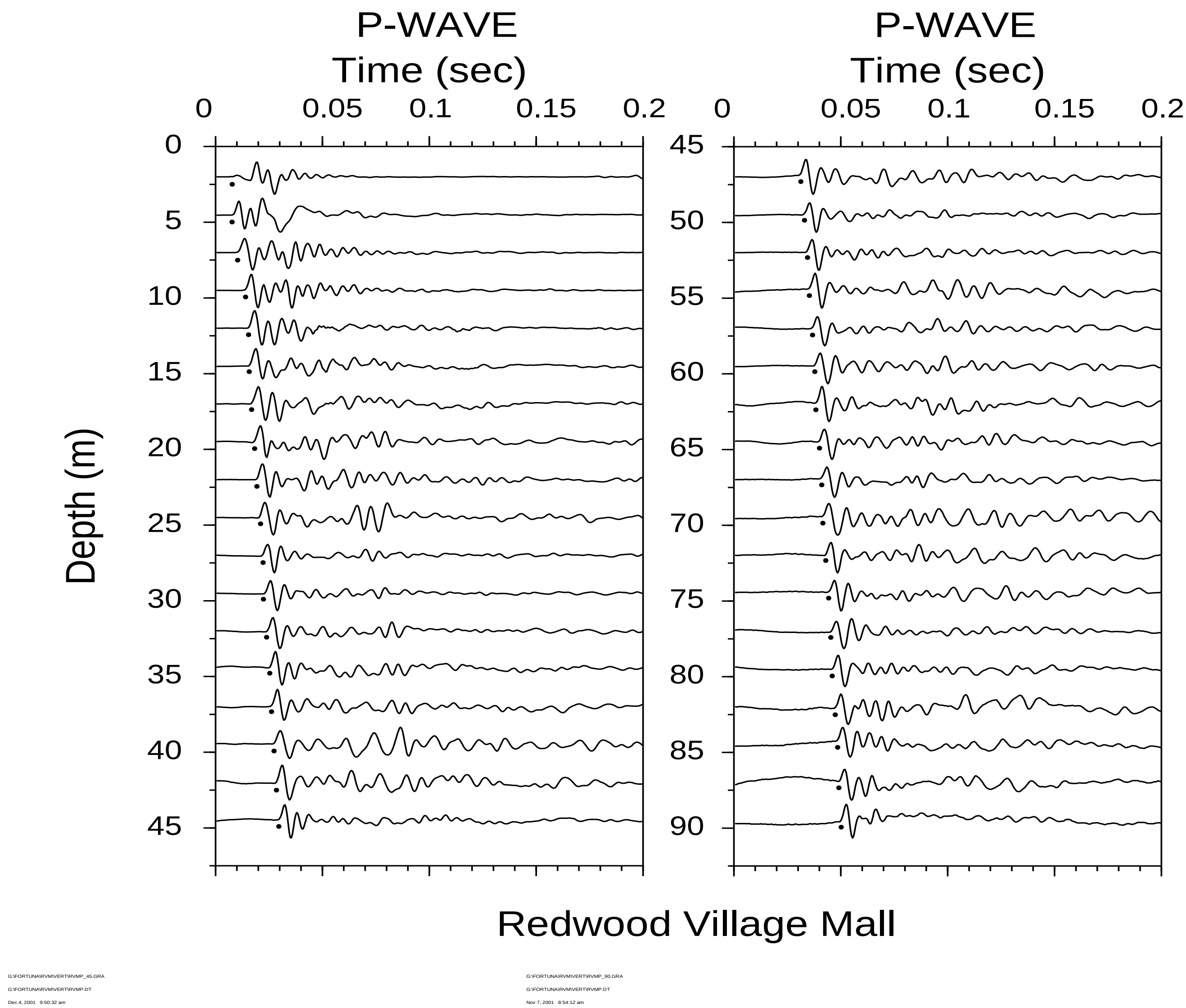

Figure A-18. Vertical component record section. Approximate P-wave arrivals are indicated by the dots.

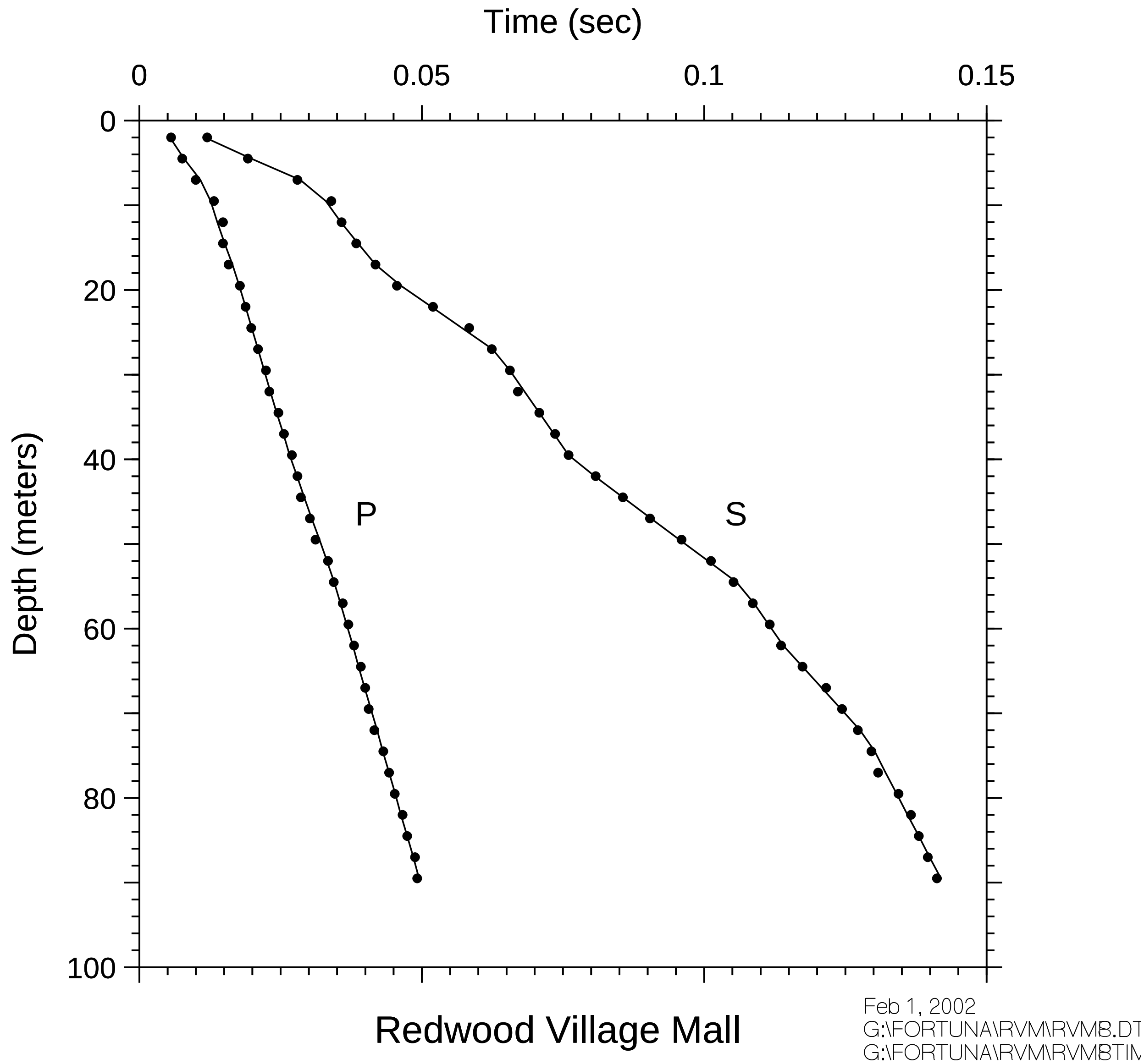

Figure A-19. Time-depth graph of P-wave and S-wave picks. Line segments are straightline interpolations of model predictions at the observation depths. The times for zero depth, not shown, are given by the horizontal offset ($hoffset$) divided by the velocity in the uppermost layer (see accompanying tables of velocities for specific values).

34

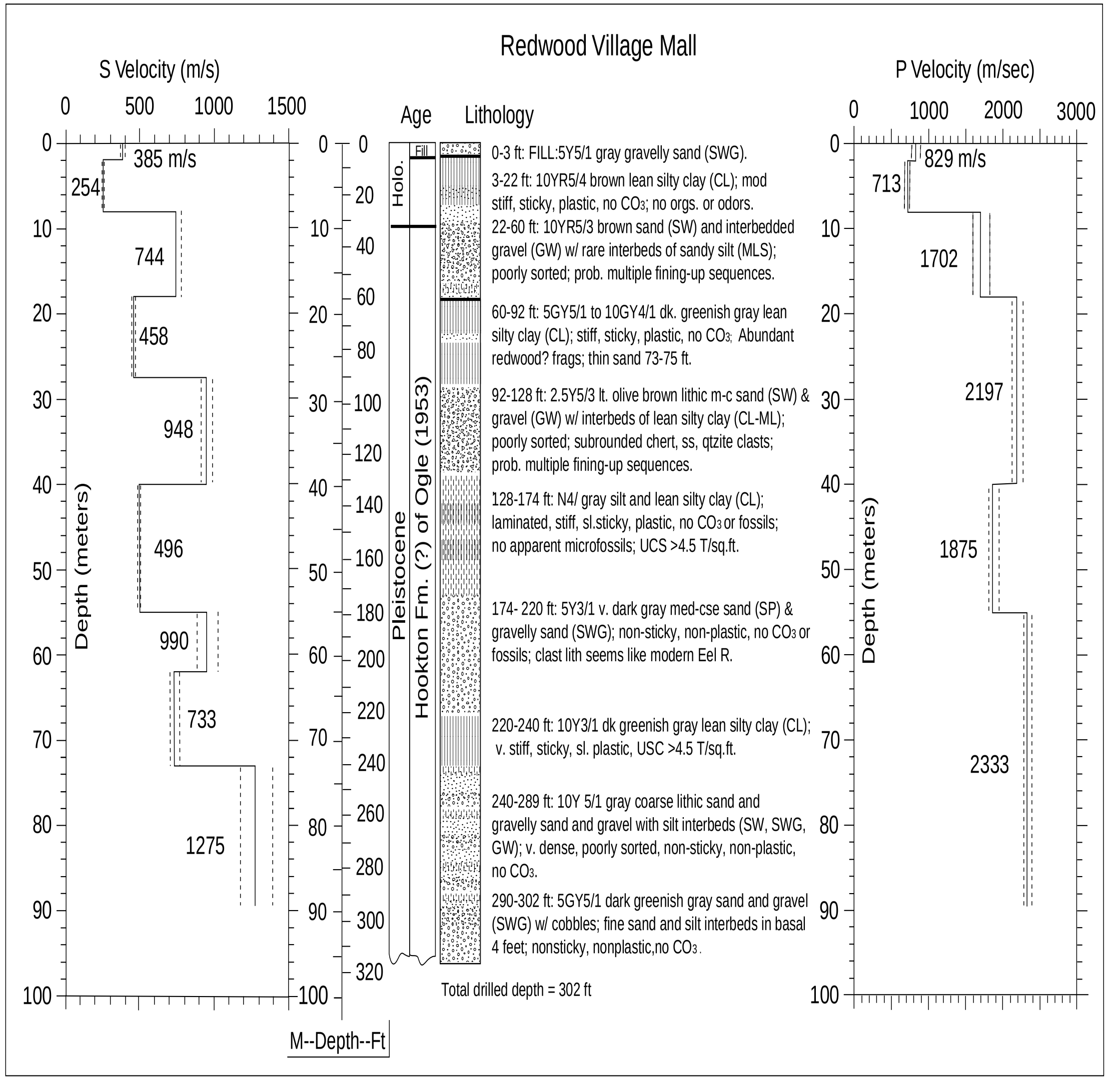

Figure A-20. S- and P-wave velocity profiles with lithology. Dashed lines represent plus and minus one standard deviation of velocities.

Figure A-21. Site location map for the borehole at Rio Dell. The highway (US 101) has been rerouted and is close to the borehole. The accelerograph is located approximately 10 meters from the borehole.

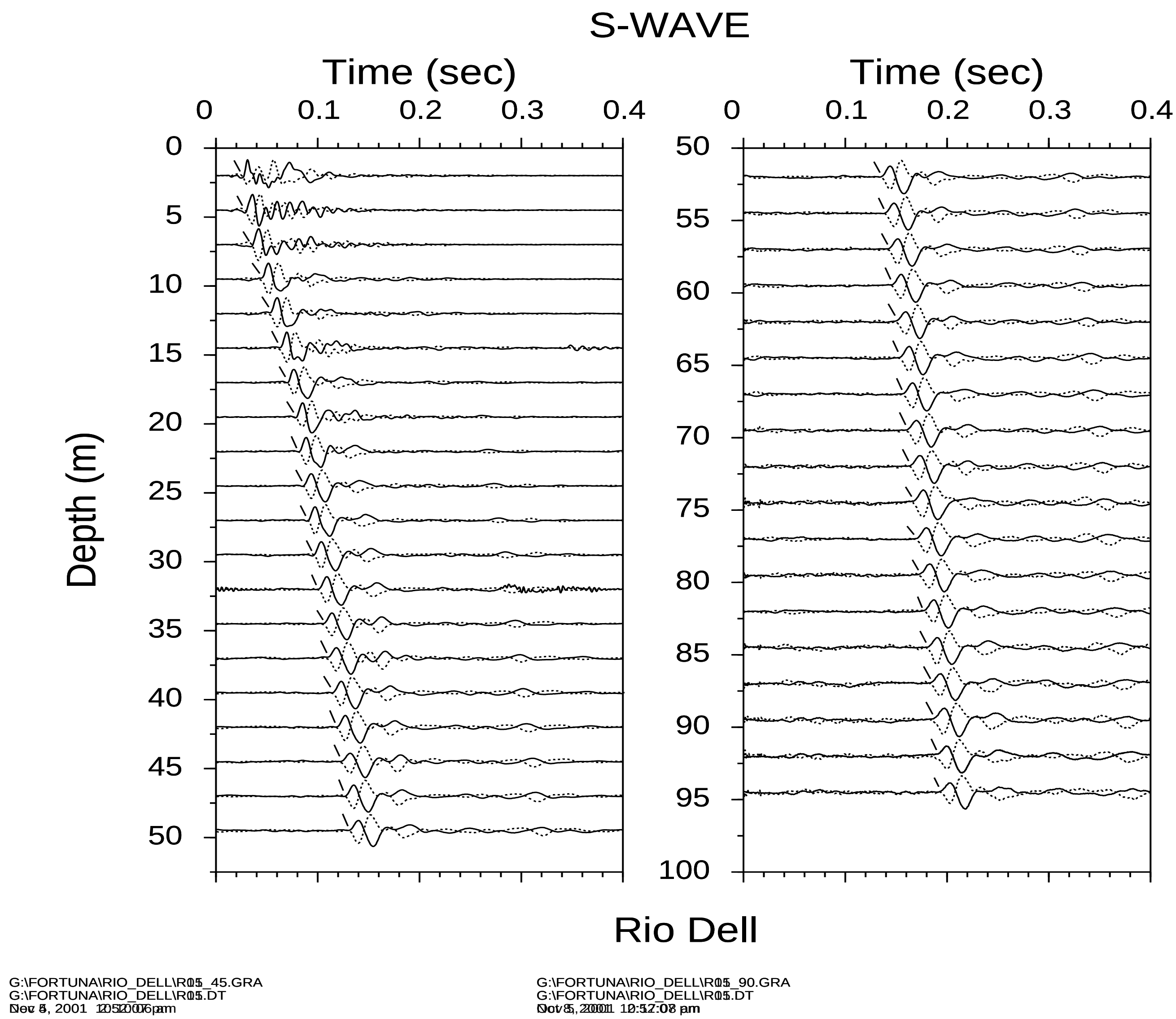

Figure A-22. Horizontal component record section (from impacts in opposite directions) superimposed for identification of S-wave onset. Approximate S-wave time picks are indicated by the hatch marks.

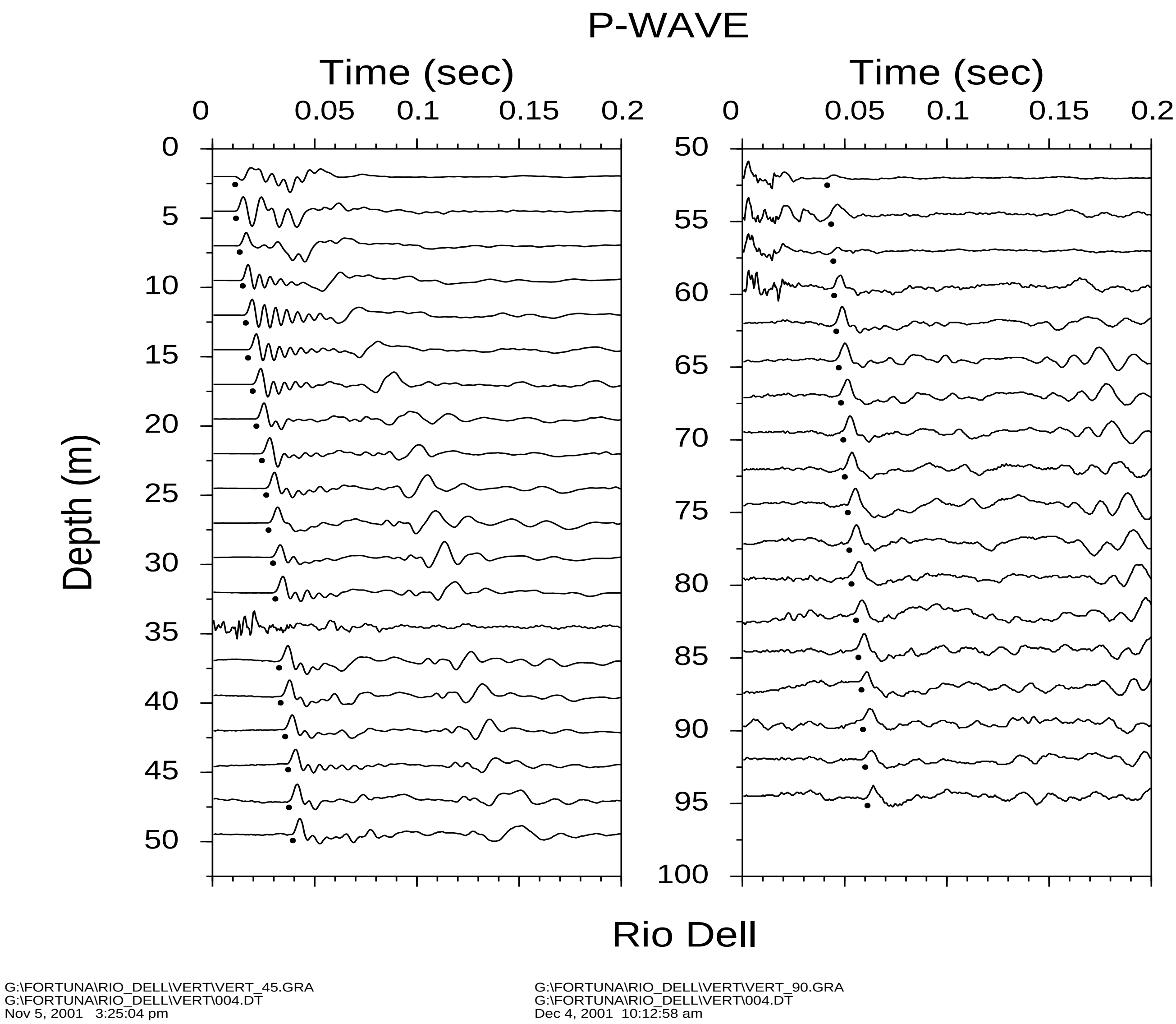

Figure A-23. Vertical component record section. Approximate P-wave arrivals are indicated by the dots.

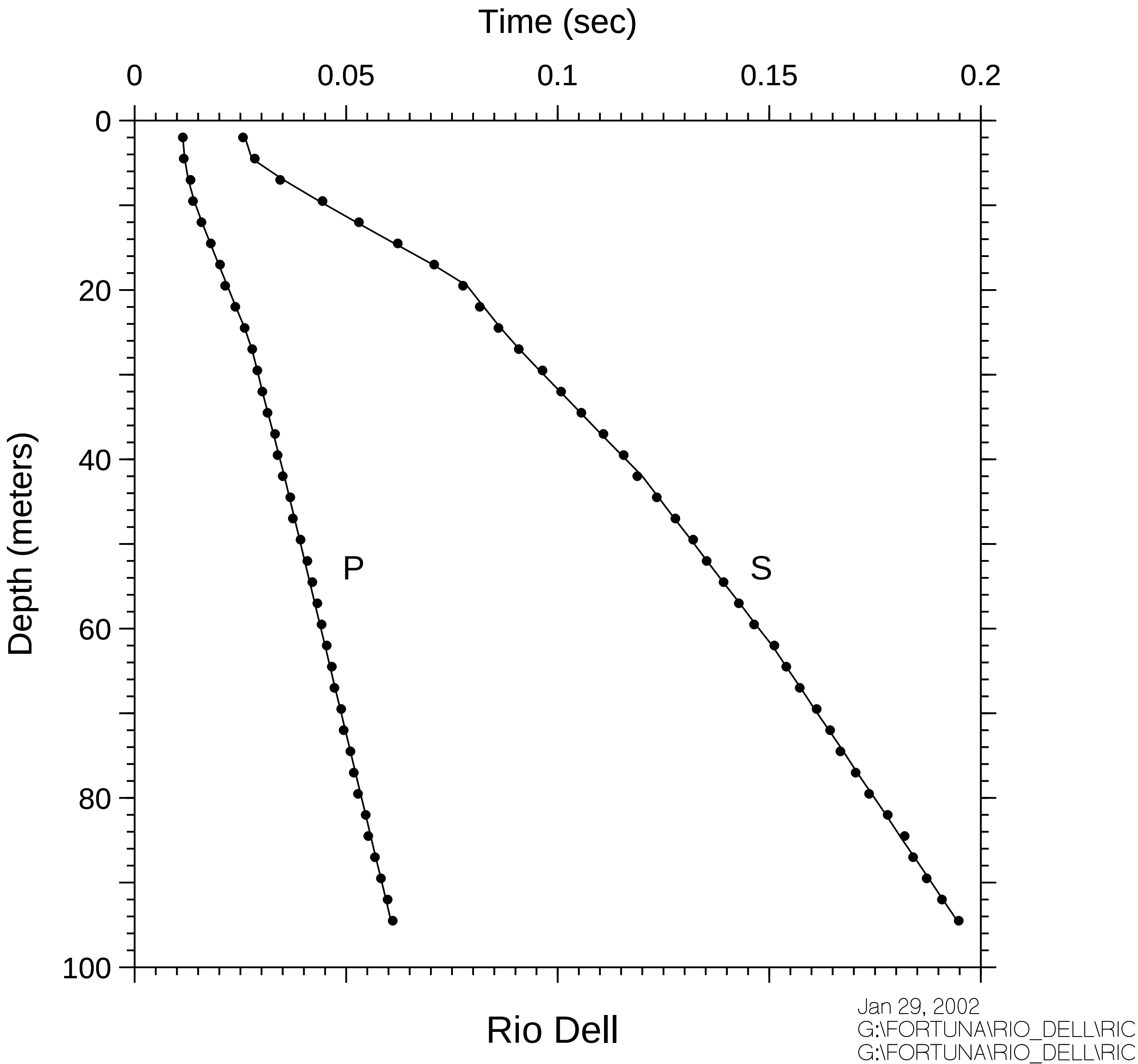

Figure A-24. Time-depth graph of P-wave and S-wave picks. Line segments are straightline interpolations of model predictions at the observation depths. The times for zero depth, not shown, are given by the horizontal offset ($hoffset$) divided by the velocity in the uppermost layer (see accompanying tables of velocities for specific values).

41

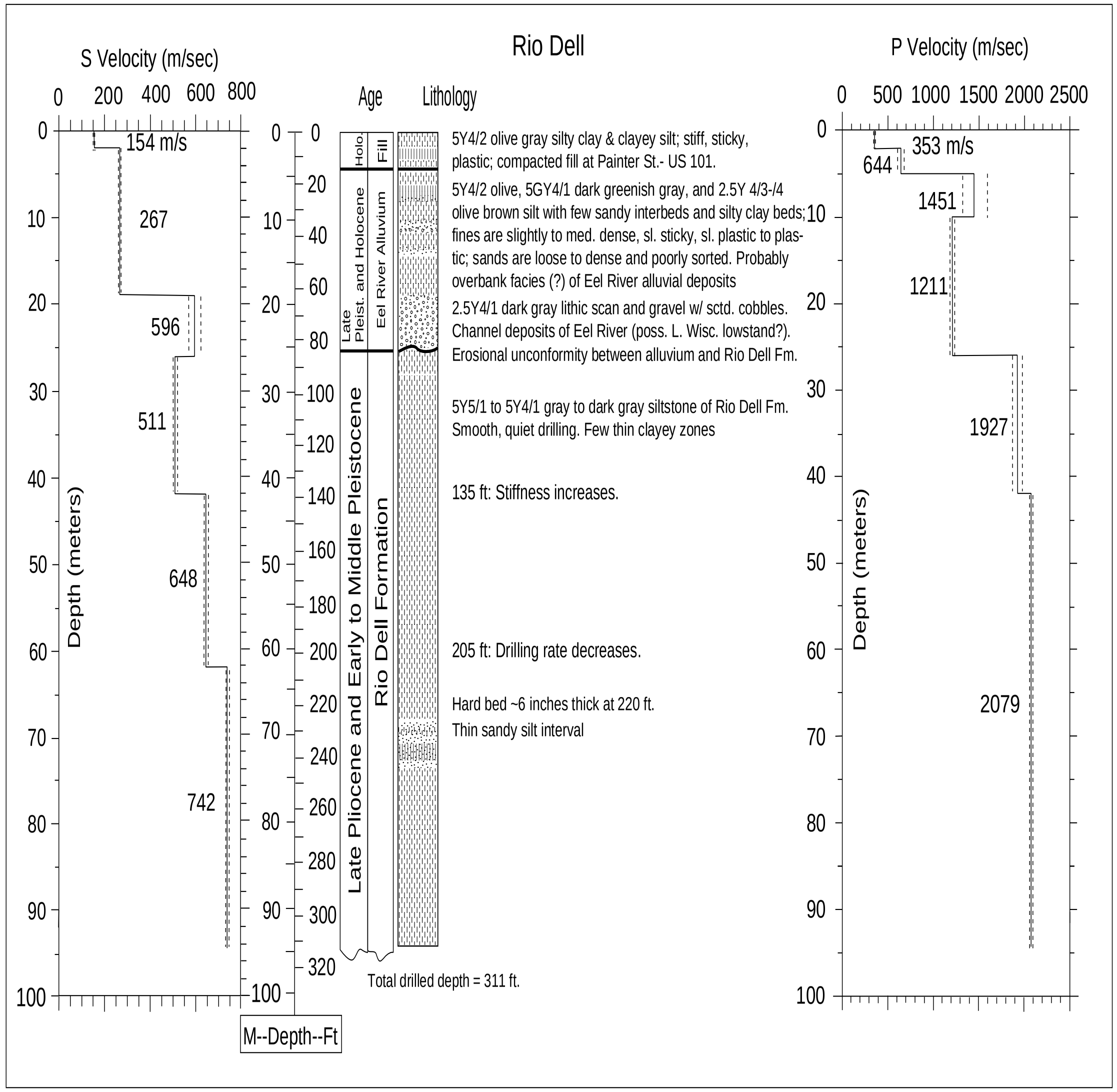

Figure A-25. S- and P-wave velocity profiles with lithology. Dashed lines represent plus and minus one standard deviation of velocities.

APPENDIX—B

Poisson's Ratios